Journal of Non-Crystalline Solids 608 (2023) 122251

Contents lists available at ScienceDirect

Journal of Non-Crystalline Solids

journal homepage: www.elsevier.com/locate/jnoncrysol

Thermal insulation of 3D printed complex and miniaturized SiO_2 aerogels at medium-high temperatures

Yuting Wang [a,b], Chengyi Chu [b], Chenqi Duan [b], Jiajing Dong [b], Hao Chen [b], Songtao Ying [b], Jianjun Guo [b], Gaojie Xu [b], Fang Hu [a], Yuchuan Cheng [b,*], Aihua Sun [b,*]

[a] School of Materials Science and Chemical Engineering, Ningbo University, Ningbo 315211, PR China
[b] Key Laboratory of Additive Manufacturing Materials of Zhejiang Province, Ningbo Institute of Materials Technology and Engineering, Chinese Academy of Science, Ningbo 315201, PR China

ARTICLE INFO

Keywords:
3D printing
SiO_2 aerogel
Opacitiers
Thermal insulation
Medium-high temperatures

ABSTRACT

Due to aerogel's network structure, specific surface area, and high porosity, SiO_2 aerogel has excellent thermal insulation and inferior mechanical properties. It is challenging to produce micro-objects and complex-shaped objects accurately by traditional manufacturing method because of the fragile mechanical properties. Here, we use 3D printing to fabricate SiO_2 aerogels. At the same time, we add opacifiers to reduce the aerogel's medium-high temperature thermal conductivity. The thermal conductivity of the SiO_2 aerogel printed in the experiment is as low as 0.028 W/(m·K) at room temperature. The aerogel doped with 10 wt% SiC has the best thermal insulation at medium-high temperatures. And the 3D printed aerogel doped with 10 wt% SiC has a compression performance of 1.19 MPa, which is more than 10 times better than the usual aerogel. This paper provides a method for creating micro-objects and complex-shaped objects with excellent medium-high temperature thermal insulation using Direct Ink Writing (DIW).

1. Introduction

SiO_2 aerogels have a particular network structure of connected granules similar to a pearl necklace, with a high specific surface area, high porosity, and small average pore size [1–3]. These structures of SiO_2 aerogels provide excellent properties such as low density, low thermal conductivity, and low dielectric constant. These properties make SiO_2 aerogels superior thermal insulation materials, so SiO_2 aerogels have wide applications in aerospace [4], construction materials [5,6], protective clothing [7], etc. However, the high porosity makes the SiO_2 aerogel easy to fracture [8,9]. The preparation of SiO_2 aerogels by conventional methods cannot meet the requirements of fine shape design and high-precision manufacturing for advanced functional applications, especially for miniaturized and special-shaped objects. In this work, we use a new formation method - additive manufacturing - to shape miniaturized and heterogeneous SiO_2 aerogel samples. [8–10]. Additive manufacturing [11–14], also known as 3D printing, is a new manufacturing and processing process of "bottom-up" material accumulation. Compared with subtractive processing of traditional processing techniques, 3D printing is a technology that constructs objects by printing layer by layer. It avoids the cutting process of traditional manufacturing, does not require molds or secondary processing, is fast and efficient, and has low processing costs and high freedom. The combination of 3D printing and computer can realize batch processing and remote control of samples, and 3D printing technology has unique advantages in printing complex and miniaturized components. So 3D printing has wide applications in aerospace [15,16], medical [17,18], automobile [16,19], architecture [20], etc. Direct write printing (DIW) is the most common type of 3D printing and is available in a wide range of materials, including plastics, rubber, metals, ceramics, etc. Zhao [10] et al. used the DIW method to prepare various SiO_2 aerogel objects with high precision and shape fidelity, including honeycomb, lotus, 3D lattice, and continuous multilayer films. Moreover, the printed SiO_2 aerogel objects have ultra-low thermal conductivity, high mesoporosity, and complex geometries. These will enable the application of miniaturized SiO_2 aerogels and open up new possibilities for thermal management. Wang et al [8,9]. present a thermal-solidifying 3D printing strategy to create SiO_2 aerogels with low density, high mesoporous surface area, low thermal conductivity, and thermal stability.

At the same time, pure SiO_2 aerogels are almost transparent under

* Corresponding authors.
E-mail addresses: ycheng@nimte.ac.cn (Y. Cheng), sunaihua@nimte.ac.cn (A. Sun).

https://doi.org/10.1016/j.jnoncrysol.2023.122251
Received 15 December 2022; Received in revised form 20 February 2023; Accepted 23 February 2023

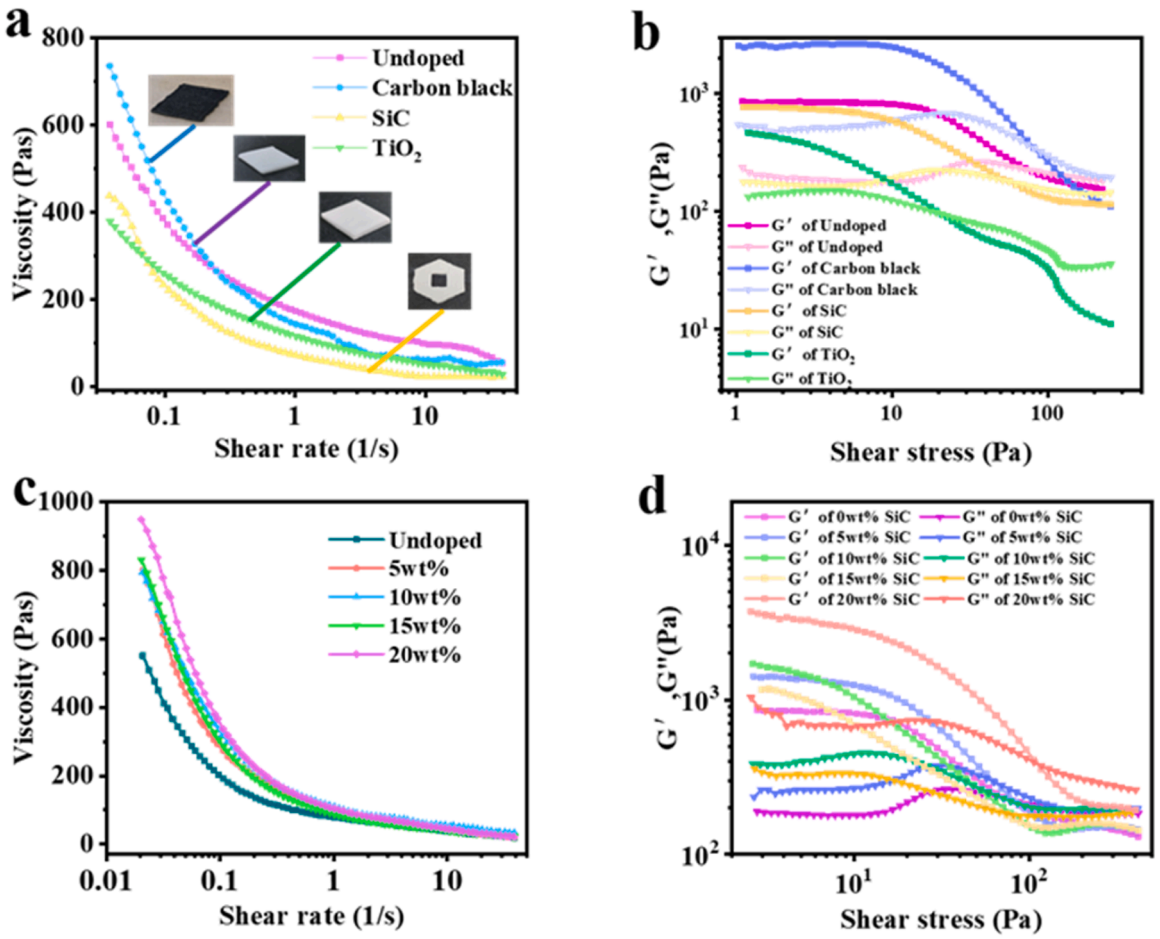

Fig. 1. Rheological properties of SiO_2 aerogel inks containing different types and contents of opacifiers. (a) Viscosity curves of printing inks containing various kinds of opacifiers. (b) G′ and G" of printing inks containing different types of opacifiers. (c) Viscosity curves of printing inks containing additional SiC content. (d) G′ and G" of printing inks containing different SiC content.

the near-infrared radiation of 2–8 μm. In contrast, the radiation is mainly infrared at temperatures above 300 K, and the primary mode of heat transfer is radiation heat transfer at medium-high temperatures. Therefore, SiO_2 aerogels have poor medium-high temperature thermal insulation performance [21–23]. Opacifiers have strong scattering and absorbing effects on radiation. The addition of the appropriate type and content of opacifier can increase the extinction coefficient, reduce the thermal conductivity of medium-high temperature radiation and improve its medium-high temperature thermal insulation performance [23,24]. Zhang et al [25]. doped SiC, ZrO_2 opacifiers, and fibers into SiO_2 aerogels and successfully improved their high-temperature thermal insulation properties. Pang et al [26]. investigated the thermal insulation properties of SiO_2 aerogels doped with SiC opacifiers. The selection of suitable opacifiers and preparation methods has been a hot topic of research. Still, most articles only investigate one of the best types and contents of opacifiers. And the method used is mostly infiltration which limit the shape of the aerogels. 3D printing is excellent for the preparation of samples with multiple materials and complex shapes, and there are few studies on the formation of SiO_2 aerogels from DIW at medium-high temperatures.

3D printing provides a new method for obtaining custom-designed SiO_2 aerogels in this paper. We investigate the rheological properties of printing inks and successfully configure inks suitable for printing. And we present DIW printing to create miniaturized and complex SiO_2 aerogel. These enable the SiO_2 aerogel to achieve directional insulation against heat, protect heat-sensitive components, and limit local temperatures in a limited space. The SiO_2 aerogels improve medium-high temperature thermal insulation properties by adding infrared opacifiers. This paper investigates the effect of different types and contents of opacifiers on the thermal conductivity of SiO_2 aerogels. The result is that SiO_2 aerogels have excellent thermal and mechanical properties at medium-high temperatures. Therefore, 3D printing aerogels doped with opacifiers can be applied in medium-high temperature insulation fields requiring miniature and complex shapes. For example, it is often necessary to insulate between them to prevent the thermal runaway of a single battery pack in a new energy vehicle from affecting the entire battery pack. 3D printing aerogels can protect the battery packs by printing complex shapes that fit accordingly to their condition. These dramatically expand the field of application of aerogels.

2. Experimental Section

2.1. Materials

In the experiment, we use deionized water as the solute, SiO_2 aerogel powder (Shenzhen Aerogel Technology Co., China) as the solute, polyvinyl alcohol (Shanghai Yingjia Industrial Development Co., China) as the binder, Tween 80 (Aladdin, China) as the dispersant, hydroxypropyl methylcellulose (Shijiazhuang Chuangsheng Building Materials Technology Co (China) as a thickener to make a slurry for printing SiO_2 aerogels. The material composition of the 3D printing paste is SiO_2 aerogel, PVA, NaC_{18}, Tween 80, and HPMC. And the material ratios are shown in Table 1. We add several different opacifiers to the printing slurry, such as SiC (Macklin, China), TiO_2 (Aladdin, China), and carbon

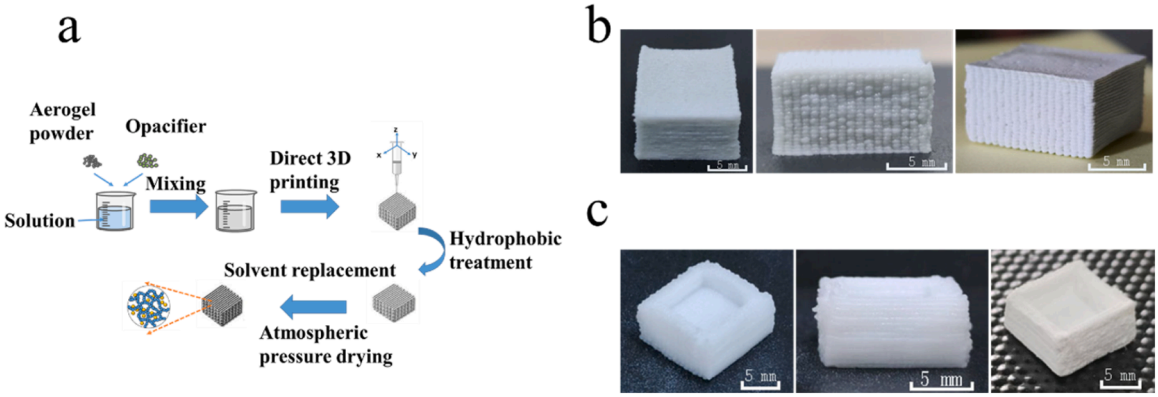

Fig. 2. Aerogel printing flow chart and printed samples. (a) Flow chart of the preparation of SiO_2 aerogel. (b) The physical image of a rectangular body printed by SiO_2 aerogel containing 10 wt% SiC opacifier. (c) Physical diagram of a hollow cuboid without a lid printed by pure SiO_2 aerogel.

black (Shandong Wanhua Tianhe New Material Co., Ltd., China). The particle size of silica aerogel is 20–50 nm, the particle size of TiO_2 is 100–400 nm, the particle size of SiC is 1-2 μm and the particle size of carbon black is 50–200 nm. The molecular weight of hydroxypropyl methylcellulose is 86000 and the molecular weight of Tween 80 is 834.

2.2. Preparation of SiO_2 Aerogel Printing Inks

First, we add 4.0 g of PVA solution (10 wt%), 0.4 g of sodium stearate, 0.14 g of Tween 80, and 0.07 g of hydroxypropyl methylcellulose using water as solvent. Tween 80 and hydroxypropyl methylcellulose are dispersants and tackifiers. Then stir at 1500 rpm/min for 120 s to obtain uniform inks. Finally, we obtain inks by mixing 4.3 g of SiO_2 aerogel powder at a speed of 1500 rpm/min for 240 s. The preparation of aerogel printing inks containing opacifiers is similar to the preparation of SiO_2 aerogel printing inks. Just add opacifiers of different types and contents before the first mixing.

2.3. Samples Printing Process

The prepared inks are loaded into a 5ml or 10ml syringe with a 0.38 mm conical needle and a 3D bio-printer (3D Bio-Architect® Sparrow, Hangzhou Regenove Biological Technology Co., Ltd., China) is used to print different models. Firstly, we create a print model using 3D modeling software and then import it into the computer. Then determine the print model and the print parameters. Select the appropriate print pressure and print speed to generate a print path for printing. Adjust the print pressure and print speed at the right time during printing.

2.4. Post-processing after printing

The printed samples also need to undergo some post-treatment, namely hydrophobic treatment, two-stage solvent replacement, and staged atmospheric pressure drying. We placed the printing samples in a hydrophobic solution for hydrophobic treatment after finishing the print. A two-stage solvent replacement followed the hydrophobic treatment. After the two-stage solvent replacement, the samples are dried at room temperature and pressure for 12 h, then dried in a drying oven at 100°C. Finally, we can gain the printed SiO_2 aerogel samples.

2.5. Characterization

The rheological characterization of the printing inks is carried out using a rotational rheometer (HAAKE R6000, Thermo Electron (Karlsruhe) GmbH, Germany). The instrument measures the viscosity of printing inks with shear rate at rates from 0.01 to 50 s^{-1} for different opacifiers types (Undoped, SiC, TiO_2, carbon black) and content (0, 5, 10, 15, 20 wt%). The storage (G′) and loss (G″) moduli are measured in the shear stress range of 1−500 Pa at a constant frequency. The compression performance tests use a 30 KN universal material testing machine (Zwick/Roell Z030, ZwickRoell GmbH & Co.KG, Germany) with a compression speed of 0.5 mm/min. The thermal conductivity measurements use a laser thermal conductivity meter (LFA467, NETZSCH, Germany). The microscopic morphology of the samples is obtained by scanning electron microscopy (SEM, Hitachi, Japan). Measure the surface area and pore diameter with the fully automated specific surface area and microporosity analyzer (ASAP2020HD88, Micromeritics, America). Infrared thermography is obtained with infrared thermal imagers (FLIR Ex, FLIR Systems, America).

3. Results and Discussions

3.1. Rheological Properties of SiO_2 Aerogel Printing Inks

The rheological natures of printing inks are essential for DIW printing, which requires both smooth extrusions of inks under pressure and certain self-supporting after printing [8,27,28]. As shown in Fig. 1a, all inks show a non-Newtonian viscoelastic behavior of shear thinning when the shear rate is 0.01–50 s^{-1}. That is, the viscosity of the inks gradually decreases with the increase of the shear rate pair. The shear thinning behavior ensures that the inks can pass through the nozzle smoothly, Respectively, Fig. 1b and 1d show the changes in storage (G′) and loss (G″) moduli of printing inks with different types and contents of opacifiers under shear stress. When the inks are stationary, or shear stress is minor, the storage (G′) and loss (G″) moduli of the inks remain relatively stable in a platform stage, and the storage moduli are greater than the loss moduli (G′>G"). The inks appear solid at this stage. With the increase of shear stress, the storage and loss moduli show a downward trend, and the storage moduli decrease slower than the loss moduli decline. The inks still appear solid at this stage. When the shear stress increases to a critical value, the storage and loss moduli are equal (G′=G"). And an intersection point appears in the rheological diagram, which is defined as the yield stress (τ_y). The inks are semi-solid. As the shear stress increases further, the loss moduli are greater than the storage moduli (G′<G"), and the inks take on a liquid state at this stage.

In Fig. 1b and d, there are intersections of storage (G′) and loss (G″) moduli. G′ and G" of different inks have platform stages. The length of the platform determines the pressure required for ink extrusion. The ink can only be extruded when the stress amplitude exceeds the platform. As the stress increases, the two curves of G′ and G" rapidly decrease and intersect [27,28]. And the inks all exhibit a high G′ platform value of 10^3–10^4, which prevents the printed object from collapsing due to gravity and the pressure exerted by the extrusion nozzle, and ensures that the printed samples are self-supported by a certain amount after the printing. These are because we add a certain amount of PVA to the inks.

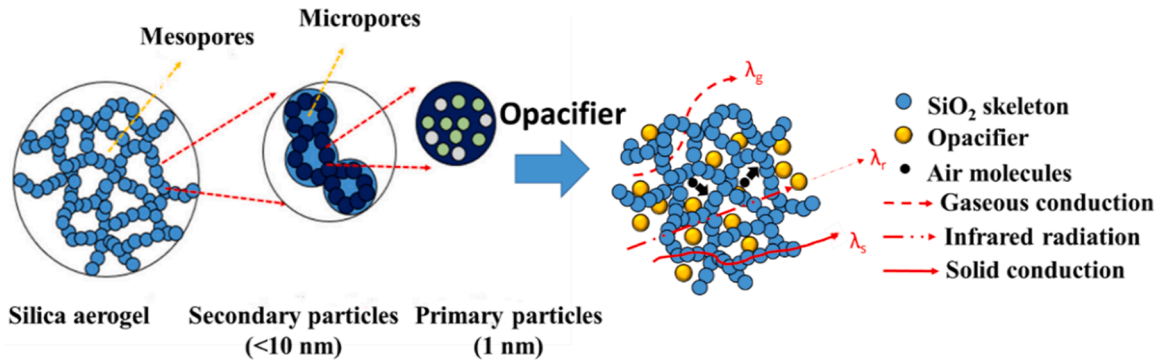

Fig. 3. Structure of aerogel and thermal insulation schematic of aerogel containing opacifiers.

PVA forms a cross-linked network structure with silica particles, which improves the viscosity of the inks and ensures smooth sample extrusion [8]. Fig. 1c shows the viscosity curve with the addition of different proportions of SiC opacifiers (0 wt%, 5 wt%, 10 wt%, 15 wt%, 20 wt%, after this referred to as 0 wt%, 5 wt%, 10 wt%, 15 wt%, 20 wt% ink). The overall curve shows a trend of shear thinning, and the viscosity of the ink increases with the increase in SiC content. The initial viscosity of 20 wt% inks is the largest, and the initial viscosity of 0 wt% inks is the smallest.

3.2. Characterization of 3D Printed SiO_2 Aerogel Samples

We use water as a solvent to add SiO_2 aerogel powder and opacifiers and stir the mixture with a planetary mixer at a speed of 1500 rpm/min to prepare printing inks. We load the inks into the print syringe and select a conical print needle of the appropriate size. Then, we determine the printing speed and printing pressure. Fig. 2b shows a sample printed with a 0.35 mm printing needle at a printing pressure of 0.15 MPa and a printing speed of 3 mm/s.

We place the printed samples in a 1:1 hydrophobic solution of methyltrimethoxysilane and ethanol for 24 h at room temperature. Because the SiO_2 aerogels without hydrophobic treatment are absorbent. Therefore, when the samples are in humid environments or air atmospheres, SiO_2 aerogels will collapse due to water absorption. The presence of water will increase the thermal conductivity of SiO_2 aerogels at room temperature, which significantly limits the application of SiO_2 aerogels [29,30]. After hydrophobic treatment, the sample needs to be dried. Standard drying methods are supercritical drying (SCD), freeze drying (FD), and atmospheric pressure drying (APD) [3,31]. We choose atmospheric pressure drying which is more convenient and inexpensive for this experiment. Therefore, we must perform a two-stage solvent displacement of the sample before drying. Firstly, place the samples in ethanol and displaced in a 60°C water bath for 24 h, then the samples are displaced in hexane for 24 h. We design the two-stage solvent replacement to replace the high surface tension solvent in the sample void with a low surface tension solvent to reduce capillary forces and avoid collapse and fragmentation of the sample due to large capillary forces during drying [32]. Finally, we obtain 3D printing SiO_2 aerogels via room temperature drying for 12 h and 100°C drying for 12 h. The linear shrinkage of the SiO_2 aerogel obtained is large and will reach 23%. The minimum density is 0.4 g/cm^3.

3.3. Thermal Conductivity Study of Printed SiO_2 Aerogel Samples

With high porosity and specific surface area, SiO_2 aerogels have excellent thermal insulation performance. The three main heat conduction modes of aerogels are solid-phase conduction, vapor-phase conduction, and radiation conduction. Due to the large specific surface area of aerogel and the long solid phase conduction path, the solid phase thermal conductivity is low. The radiative heat transfer is negligible at room temperature. Therefore, the thermal conductivity of aerogels depends mainly on the vapor-phase heat transfer at room temperature. However, due to the increase in temperature, infrared radiation enhances, and the radiant thermal conductivity increases, which makes the thermal conductivity of aerogels at medium-high temperatures significantly higher than at room temperature. To limit the thermal conductivity of aerogels at medium-high temperatures, we

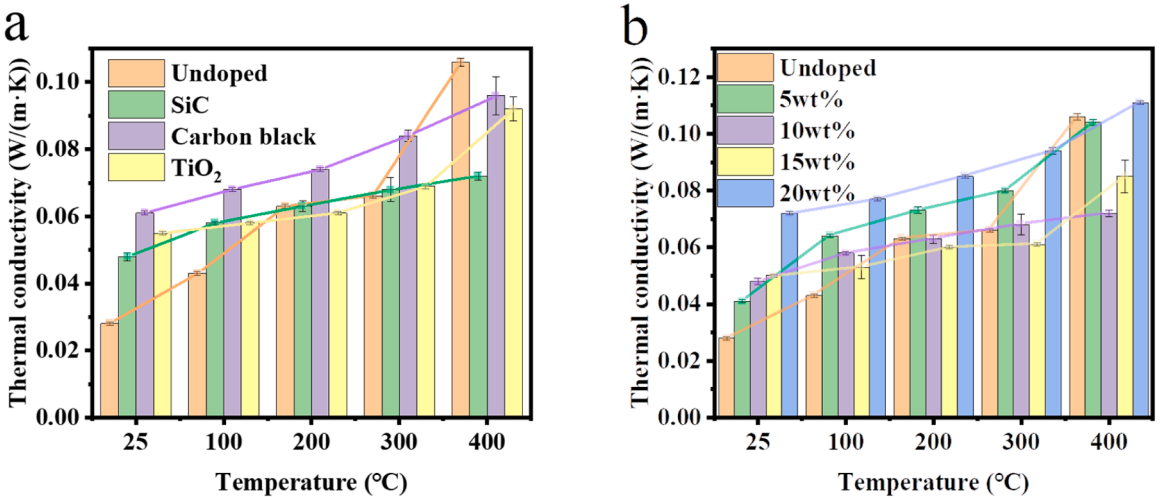

Fig. 4. Thermal conductivity of SiO_2 aerogels containing different types and contents of opacifiers at different temperatures. (a) Thermal conductivity of SiO_2 aerogels containing different kinds of opacifiers. (b) Thermal conductivity of SiO_2 aerogels containing different amounts of SiC.

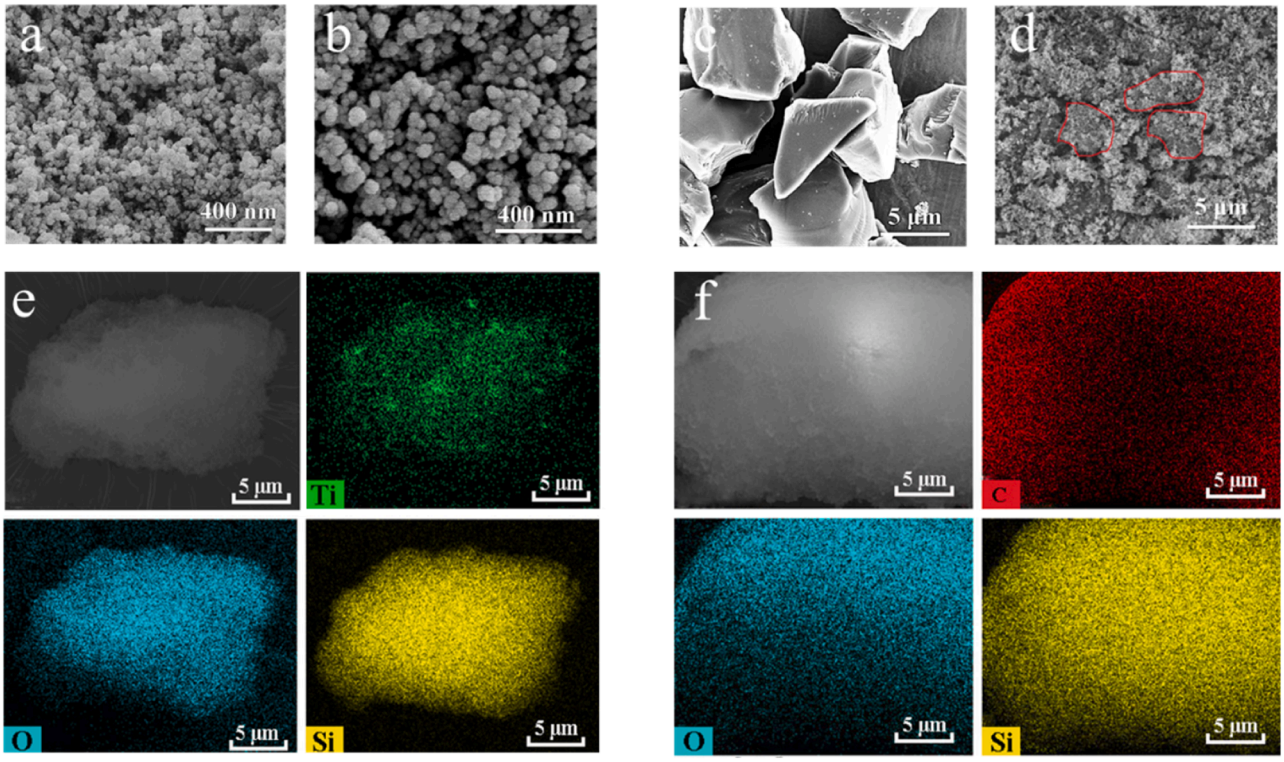

Fig. 5. Scanning electron microscopy and mapping elemental analysis pictures (a) (b) SiO_2 aerogels, (c) SiC. (d) SiC-SiO_2 aerogel. (e) TiO_2-SiO_2 aerogel mapping elemental analysis pictures, (f) the elemental analysis pictures of carbon black-SiO_2 aerogel.

add infrared opacifiers to aerogels. As shown in Fig. 3, SiO_2 aerogels have primary particles and secondary particles. The porous structure in the aerogel forms when the secondary particles connect. Due to the pacifiers' strong absorption and scattering ability to infrared radiation, the thermal conductivity of the aerogel at medium-high temperatures reduces when we add opacifiers to the aerogel. So, we use three common infrared opacifiers such as SiC, TiO_2, and carbon black in the experiments.

Here, we study infrared opacifiers' best type and content at 25 to 400°C. Fig. 4a shows the thermal conductivity of aerogels doped with 10 wt% SiC, 10 wt% TiO_2, 10 wt% carbon black opacifiers, and undoped aerogels at different temperatures (later referred to as SiC-SiO_2 aerogel, TiO_2-SiO_2 aerogel, carbon black-SiO_2 aerogel, SiO_2 aerogel). The thermal conductivity of SiO_2 aerogel at 25°C is as low as 0.028 W/(m·K). With the increase in temperature, the thermal conductivity of SiO_2 aerogels gradually increases, which has increased to 0.106 W/(m·K) at 400°C. After adding opacifiers, the thermal conductivity at room temperature increases significantly. Because the doped opacifiers will enhance the aerogel's solid-phase thermal conductivity. With the temperature increasing, the thermal conductivity of aerogels doped with different opacifiers will increase correspondingly, but the increase is slower than SiO_2 aerogels. At room temperature, a comparison of the thermal conductivity of the aerogels doped with opacifiers shows that SiC-SiO_2 aerogels have the lowest thermal conductivity, while carbon black SiO_2 aerogels have the highest thermal conductivity. When the temperature rises from 25 to 400°C, the growth of SiC-SiO_2 aerogel is the smallest. The growth of TiO_2-SiO_2 aerogel is also small between 25 and 300°C, but the thermal conductivity increases significantly from 300°C to 400°C. Combining the magnitude and increase of thermal conductivity at different temperatures, we finally chose SiC as the infrared opacifier of aerogels.

Next, we investigate the effects of different SiC content on the thermal conductivity of aerogels at different temperatures. Fig. 4b shows the thermal conductivity of doped 0 wt%, 5 wt%, 10 wt%, 15 wt%, and 20 wt% SiC at different temperatures (later referred to as SiO_2 aerogel, 5 wt%-SiO_2 aerogel, 10 wt%-SiO_2 aerogel, 15 wt%-SiO_2 aerogel, 20 wt %-SiO_2 aerogel). At 25°C, the thermal conductivity gradually increases with the increase of SiC content. Because the more SiC doped, the stronger the solid-phase conduction and the greater the thermal conductivity of the aerogel. With the rising temperatures, the thermal conductivity of aerogels with different SiC content gradually increases. When fewer opacifiers are added, the thermal conductivity of the aerogel is slight at room temperature but the thermal conductivity increases significantly at medium-high temperatures. At 400°C, the thermal conductivity of 5 wt%-SiO_2 aerogel is as high as 0.104 W/(m·K) but it is lower than that without opacifiers. When there are more doped opacifiers, the thermal conductivity of the aerogels will increase due to excessive solid doping, but when we increase the temperature, the thermal conductivity increases less. When more opacifiers are added, the thermal conductivity of the aerogels increases at room temperature, but when we increase the temperature, the thermal conductivity increases less. The thermal conductivity of 20 wt%-SiO_2 aerogel is as high as 0.072 W/(m·K) at room temperature. Still, when it increases to 400°C, the thermal conductivity is 0.111 W/(m·K), which is an increase of 54.2% compared to the thermal conductivity at room temperature. In contrast, the thermal conductivity of silica aerogel at 400°C is 0.106 W/(m·K), which is an increase of 278.6% compared to the room temperature thermal conductivity. The study comparison finds that doping opacifiers at 10 wt% show excellent medium-high temperature thermal insulation.

The thermal conductivity of SiO_2 aerogels closely relates to their microstructure. Fig. 5 shows the scanning electron microscopy (SEM) pictures of aerogels and mapping elemental analysis pictures. Fig. 5a and b are the microstructure of SiO_2 aerogels. Fig. 5a shows that the silica is a cross-linked network of pearl strand-like skeletons with many holes in the middle. Further enlarged, the SiO_2 particles are spheres with a diameter of about 20–60 nm from fig. 5b–d show the microstructure pictures of the infrared opacifiers SiC and SiC-SiO_2 aerogels, but silica

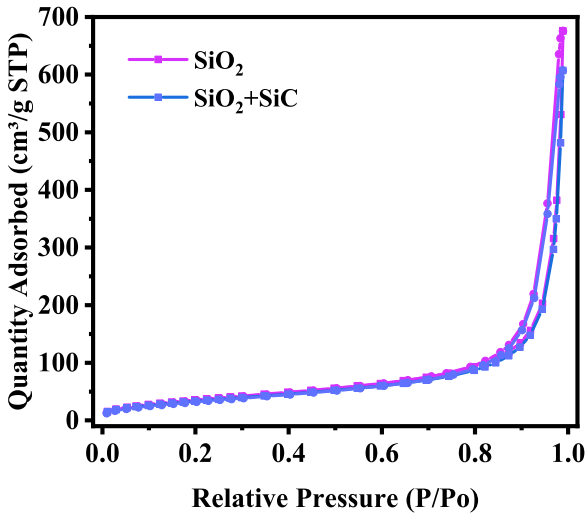

Fig. 6. Adsorption–desorption isotherms of SiO_2 and SiO_2-SiC.

particles completely cover the SiC. The TiO_2, carbon black, and silica particles are all spherical, and we can't see the doping of the opacifiers in the SEM, so we map the elemental distribution, as shown in Fig. 5e and f. Those clearly show that the main elements of TiO_2-SiO_2 aerogel and carbon black-SiO_2 aerogel are Ti, O, Si and C, O, Si. At the same time, those suggest that the aerogels successfully dope TiO_2 and carbon black.

The SEM pictures clearly show the micromorphology of the material. Nevertheless, we still need to determine the quantitative structural properties by the nitrogen adsorption method to determine the porous material's specific surface area and pore size distribution. Fig. 6 shows the adsorption–desorption isotherms. All SiO_2 aerogels have type IV isotherms. The adsorption–desorption isotherms rise slowly in the low-pressure section and take the shape of upward micro convexity, which is the transition from adsorption monolayer to multilayer. The adsorption capacity in the middle of the curve slowly increases with the increase of pressure, and this stage is the multilayer adsorption process. The adsorption line rises sharply in the second half of the curve. Moreover, there is a specific hysteresis loop when the adsorption curve does not coincide with the analytical curve, indicating pores structure in both the raw material aerogels and the printed samples. The average pore size of the SiC-SiO_2 aerogel is 24.8 nm, with the largest number of micropores less than 10 nm and a smaller number of mesopores and macropores.

We can use printed aerogels doped with opacifiers to extract the thermal insulation effects in practical applications. As shown in Fig. 7, place a 6 mm thick printed SiC-SiO_2 aerogel on a hot plate at 300°C and place a leaf on top of the aerogel. We heat the hot plate for 10 minutes and then place the aerogel on the hot plate, at which time the minimum temperature of the leaves on the aerogel is 45°C. After heating for 10 min, the minimum temperature of the leaves on the gel is 86°C. SiC-SiO_2 aerogel successfully isolates most of the heat to protect the leaf on the aerogel. Thus, SiO_2 aerogels can achieve targeted thermal insulation, protect heat-sensitive components and limit local temperatures at medium-high temperatures and in small spaces by using 3D printing. These make it possible to apply SiO_2 aerogels in new energy batteries, smartphones, optical devices, and other fields, greatly expanding the applications of SiO_2 aerogels.

3.4. *Mechanical Properties Study of Printed SiO_2 Aerogel Samples*

Due to the high porosity and specific surface area, SiO_2 aerogels have excellent thermal insulation and inferior mechanical properties. We use 3D printing molding to solve the defect of poor SiO_2 aerogel molding performance, and we can establish models through 3D modeling software and print various complex shapes accordingly. As shown in Fig. 8, in this experiment, the printed SiO_2 aerogel showed typical compression deformation behavior and linear elastic behavior at low strain, followed by yield, strain hardening, and fracture. And the compressive strength of our printed SiO_2 aerogel reaches 1.08 MPa, the compressive strength of SiC-SiO_2 reaches 1.19 MPa, and the compressive strength of the aerogel and the common pure SiO_2 aerogel is only 0.047–0.16 MPa [33]. The power of the printed SiC-SiO_2 aerogel is more than 10 times better than the common pure SiO_2 aerogel.

4. Conclusion

In summary, we successfully prepare SiO_2 aerogel printing inks containing three different opacifiers, SiC, TiO_2, carbon black, and various added contents of 0, 5, 10, 15, and 20 wt%. We investigate the rheological properties of different inks and successfully print aerogel samples with complex shapes. Then we study the thermal conductivity of the printed sample at 25°C-400°C. The results show that the thermal conductivity of the printed pure SiO_2 aerogel is as low as 0.028 W/(m·K)

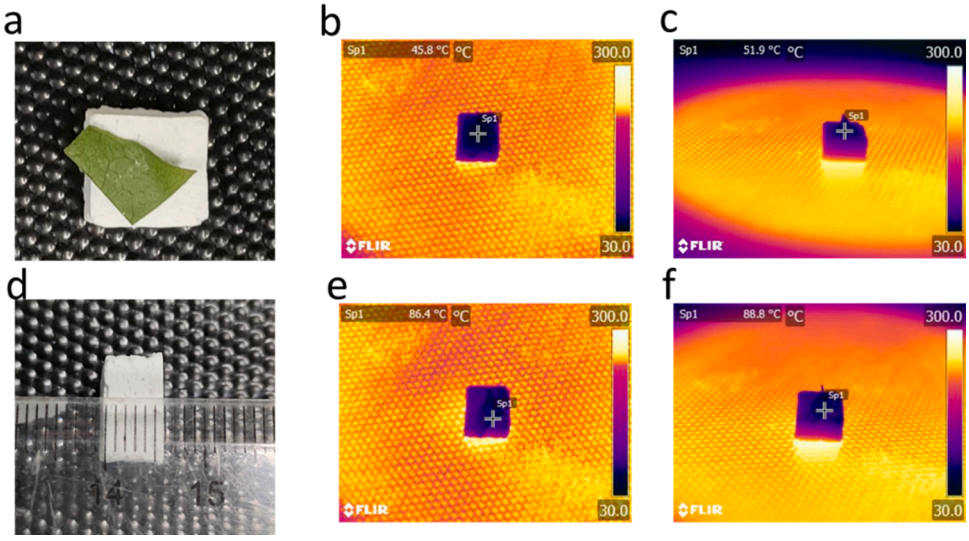

Fig. 7. Infrared thermal imaging image of aerogel heat insulation after placing 6 mm on a 300 °C base plate. (a) physical drawing, (d) the thickness of the aerogel, (b, c) the infrared thermal imaging image of the aerogel, (e, f) the infrared thermal imaging image of the aerogel after 10 min.

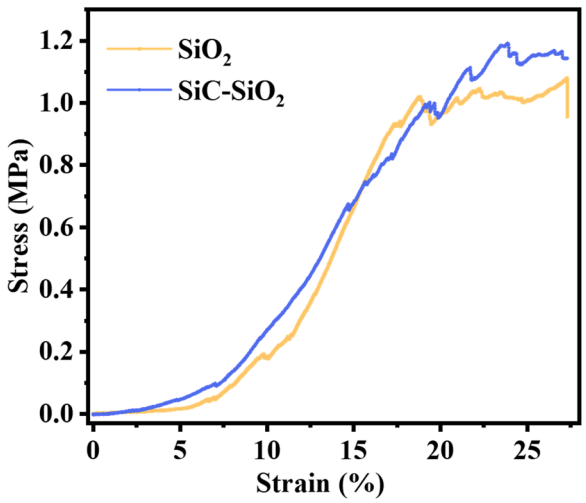

Fig. 8. Compressive stress-strain diagrams of SiO_2 aerogels and SiC-SiO_2 aerogels.

Table 1
Material ratios for printing pastes.

Materials	SiO_2 aerogel	PVA	NaC_{18}	Tween 80	HPMC
Ratios	80.98%	7.53%	7.53%	2.64%	1.32%

at 25°C, which is significantly lower than that of the aerogel doped with opacifier. The aerogel doped with 10 wt% SiC has the best medium-high temperature thermal insulation performance. At the same time, our study finds that the compression performance of aerogels doped with SiC opacifiers reaches 1.19 MPa, which is more than 10 times better than the conventional aerogels. Therefore, 3D printing offers a new way of forming SiO_2 aerogels, allowing them to achieve insulation from heat, protect heat-sensitive components and impose local temperature limits at medium to high temperatures and in limited spaces. These greatly expand aerogels' application in many fields, such as aerospace and new energy vehicle batteries.

Data availability

Data will be made available on request.

CRediT authorship contribution statement

Yuting Wang: Investigation, Formal analysis, Writing – original draft. **Chengyi Chu:** Methodology, Supervision. **Chenqi Duan:** Validation. **Jiajing Dong:** Investigation. **Hao Chen:** Investigation. **Songtao Ying:** Investigation. **Jianjun Guo:** Supervision. **Gaojie Xu:** Funding acquisition, Supervision. **Fang Hu:** Writing – review & editing. **Yuchuan Cheng:** Funding acquisition, Supervision, Methodology. **Aihua Sun:** Supervision, Methodology.

Declaration of Competing Interest

The authors declare that they have no known competing financial interests or personal relationships that could have appeared to influence the work reported in this paper.

Data availability

Data will be made available on request.

Acknowledgments

This research is supported by the National Natural Science Foundation of China (Grant No. 52273241), and the Zhejiang Provincial Natural Science Foundation of China (Grant No. LZ22E030003).

References

[1] G. Guzel-Kaya, H. Deveci, Synergistic effects of silica aerogels/xerogels on properties of polymer composites: A review, J. Ind. Eng. Chem. 89 (2020) 13–27.
[2] K.J. Lee, Y.J. Choe, Y.H. Kim, J.K. Lee, H.J. Hwang, Fabrication of silica aerogel composite blankets from an aqueous silica aerogel slurry, Ceram. Int. 44 (2018) 2204–2208.
[3] T. Linhares, M.T. Pessoa de Amorim, L. Durães, Silica aerogel composites with embedded fibres: a review on their preparation, properties and applications, J. Mater. Chem. A 7 (2019) 22768–22802.
[4] J.P. Randall, M.A. Meador, S.C. Jana, Tailoring mechanical properties of aerogels for aerospace applications, ACS Appl. Mater. Interfaces 3 (2011) 613–626.
[5] G. Shanmugam, E. Gunasekaran, R.S. Karuppusamy, R. Ramesh, P. Vellaichamy, Utilization of aerogel in building construction –A Review, IOP Conf. Ser. Mater. Sci. Eng. 955 (2020) 257–262.
[6] A. Slosarczyk, A. Vashchuk, L. Klapiszewski, Research development in silica aerogel incorporated cementitious composites-a review, in: Polymers, 14, 2022. Basel.
[7] D. Huang, C. Guo, Thermal protective performance under fire conditions of silica aerogel felt-bedded firefighters' protective clothing, Mater. Sci. 23 (2017) 335–341.
[8] L. Wang, J. Feng, Y. Luo, Z. Zhou, Y. Jiang, X. Luo, L. Xu, L. Li, J. Feng, Three-dimensional-printed silica aerogels for thermal insulation by directly writing temperature-induced solidifiable inks, ACS Appl. Mater. Interfaces 13 (2021) 40964–40975.
[9] J. Yang, H. Wang, B. Zhou, J. Shen, Z. Zhang, A. Du, Versatile direct writing of aerogel-based sol-gel inks, Langmuir 37 (2021) 2129–2139.
[10] S. Zhao, G. Siqueira, S. Drdova, D. Norris, C. Ubert, A. Bonnin, S. Galmarini, M. Ganobjak, Z. Pan, S. Brunner, G. Nyström, J. Wang, M.M. Koebel, W.J. Malfait, Additive manufacturing of silica aerogels, Nature 584 (2020) 387–392.
[11] P. Blyweert, V. Nicolas, V. Fierro, A. Celzard, 3D printing of carbon-based materials: a review, Carbon 183 (2021) 449–485.
[12] M.N. Nadagouda, M. Ginn, V. Rastogi, A review of 3D printing techniques for environmental applications, Curr. Opin. Chem. Eng. 28 (2020) 173–178.
[13] D. Srinivasan, M. Meignanamoorthy, M. Ravichandran, V. Mohanavel, S. V. Alagarsamy, C. Chanakyan, S. Sakthivelu, A. Karthick, T.R. Prabhu, S. Rajkumar, C.R. Rambo, 3D printing manufacturing techniques, materials, and applications: an overview, Adv. Mater. Sci. Eng. 2021 (2021) 1–10.
[14] F. Zhang, Z. Li, M. Xu, S. Wang, N. Li, J. Yang, A review of 3D printed porous ceramics, J. Eur. Ceram. Soc. 42 (2022) 3351–3373.
[15] Y. Chen, Q. Wang, C. Wang, P. Gong, Y. Shi, Y. Yu, Z. Liu, Topology optimization design and experimental research of a 3D-printed metal aerospace bracket considering fatigue performance, Appl. Sci. 11 (2021), 6671.
[16] C.W.J. Lim, K.Q. Le, Q. Lu, C.H. Wong, An overview of 3-d printing in manufacturing, aerospace, and automotive industries, IEEE Potentials 35 (2016) 18–22.
[17] M.N. Nadagouda, V. Rastogi, M. Ginn, A review on 3D printing techniques for medical applications, Curr. Opin. Chem. Eng. 28 (2020) 152–157.
[18] Z. Wang, Y. Yang, Application of 3D printing in implantable medical devices, Biomed. Res. Int. 2021 (2021), 6653967.
[19] M. Schmitt, R.M. Mehta, I.Y. Kim, Additive manufacturing infill optimization for automotive 3D-printed ABS components, Rapid Prototyp. J. 26 (2020) 89–99.
[20] P. Bedarf, A. Dutto, M. Zanini, B. Dillenburger, Foam 3D printing for construction: A review of applications, materials, and processes, Autom. Constr. 130 (2021), 103861.
[21] H. Liu, J.a. Liu, Y. Tian, X. Wu, Z. Li, Investigation of high temperature thermal insulation performance of fiber-reinforced silica aerogel composites, Int. J. Therm. Sci. 183 (2023), 107827.
[22] V.G. Parale, H.N.R. Jung, W. Han, K.Y. Lee, D.B. Mahadik, H.H. Cho, H.H. Park, Improvement in the high temperature thermal insulation performance of Y2O3 opacified silica aerogels, J. Alloys Compd. 727 (2017) 871–878.
[23] C.Y. Zhu, Z.Y. Li, H.Q. Pang, N. Pan, Design and optimization of core/shell structures as highly efficient opacifiers for silica aerogels as high-temperature thermal insulation, Int. J. Therm. Sci. 133 (2018) 206–215.
[24] H. Zhang, W.Z. Fang, X. Wang, Y.M. Li, W.Q. Tao, Thermal conductivity of fiber and opacifier loaded silica aerogel composite, Int. J. Heat Mass Transf. 115 (2017) 21–31.
[25] H. Zhang, C. Zhang, W. Ji, X. Wang, Y. Li, W. Tao, Experimental characterization of the thermal conductivity and microstructure of opacifier-fiber-aerogel composite, Molecules 23 (2018), 2198.
[26] P. Hao-Qiang, L. Zeng-Yao, Experimental investigations on the thermal insulation performance of SiC opacifier doped silica aerogel at large temperature difference, Int. J. Therm. Sci. 160 (2021), 106681.
[27] Z. Ye, C. Chu, D. Zhang, S. Ma, J. Guo, Y. Cheng, G. Xu, Z. Li, A. Sun, Study on 3D-Direct Ink Writing based on adding silica submicron-particles to improve the rheological properties of alumina ceramic ink, Mater. Today Commun. 28 (2021), 102534.

[28] D. Zhang, C. Chu, S. Ma, Y. Wang, C. Duan, J. Guo, X. Shi, G. Xu, Y. Cheng, A. Sun, A novel method to avoid the sintering shrinkage of Al2O3-Cr cermets formed by direct ink writing, J. Alloys Compd. 931 (2023), 167632.
[29] A.M. Anderson, M.K. Carroll, Hydrophobic Silica Aerogels: Review of Synthesis, Properties and Applications, Aerogels Handbook, 2011, pp. 47–77.
[30] Y. Duan, S.C. Jana, B. Lama, M.P. Espe, Hydrophobic silica aerogels by silylation, J. Non-Cryst. Solids 437 (2016) 26–33.
[31] J. Wang, D. Petit, S. Ren, Transparent thermal insulation silica aerogels, Nanoscale Adv. 2 (2020) 5504–5515.
[32] V.V. Ganbavle, A.S. Kalekar, N.S. Harale, S.S. Patil, S.L. Dhere, Rapid synthesis of ambient pressure dried tetraethoxysilane based silica aerogels, J. Sol Gel Sci. Technol. 97 (2020) 5–10.
[33] J. Fu, C. He, J. Huang, Z. Chen, S. Wang, Cellulose nanofibril reinforced silica aerogels: optimization of the preparation process evaluated by a response surface methodology, RSC Adv. 6 (2016) 100326–100333.